On the potential of Cluster Ion Counter (CIC) to observe local new particle formation, condensation sink and growth rate of newly formed particles

Markku Kulmala[1,2,3], Santeri Tuovinen[1], Sander Mirme[4,5], Paap Koemets[4,5], Lauri Ahonen[1], Yongchun Liu[2], Heikki Junninen[.4], Tuukka Petäjä[1,2,3] and Veli-Matti Kerminen[1]

[1] Institute for Atmospheric and Earth System Research (INAR)/Physics, University of Helsinki, Helsinki, 00014, Finland
[2] Aerosol and Haze Laboratory, Beijing Advanced Innovation Center for Soft Matter Science and Engineering, Beijing University of Chemical Technology, Beijing, 100089, China
[3] Joint International Research Laboratory of Atmospheric and Earth System Sciences, School of Atmospheric Sciences, Nanjing University, Nanjing, 210023, China
[4] Institute for Physics, University of Tartu, Tartu, 50090, Estonia
[5] Airel Ltd., Observatooriumi 5, 61602 Tõravere, Estonia

Correspondence to: Markku Kulmala (markku.kulmala@helsinki.fi)

Abstract

Cluster Ion Counter (CIC) is a simple 3-channel instrument designed to observe ions in the electrical mobility equivalent diameter range from 1.0 to 5 nm. With the three channels, we can observe concentrations of both ion clusters (sub-2 nm ions) and intermediate ions. Furthermore, as derived here, we can estimate condensation sink (CS), intensity of local new particle formation, growth rate of newly formed particles from 2 nm to 3 nm, and formation rate of 2 nm ions. We compared CIC measurements with those of a multichannel ion spectrometer, the Neutral cluster and Air Ion Spectrometer (NAIS), and found that the concentrations agreed well between the two instruments, with the correlation coefficients of 0.89 and 0.86 for sub-2 nm and 2.0–2.3 nm ions, respectively. According to the observations made in Hyytiälä, Finland and Beijing, China, the ion source rate was estimated to be about 2–4 ion pairs cm^{-3} s^{-1}. The new CIC is a simple and cheap instrument that can be used in different environments to obtain information about small ion dynamics, local intermediate ion formation and CS in a robust way when combined with the theoretical framework presented here.

1. Introduction

New particle formation (NPF) is the dominant source of the number concentration of aerosol particles in the global atmosphere (Gordon et al., 2017), thereby having potentially large influences on global climate (e.g. Boucher et al., 2013) and regional air quality (e.g. Guo et al., 2014; Kulmala et al., 2022). During the past 2-3 decades, atmospheric NPF has been characterized in terms of the particle formation and growth rates at a vast variety of sites in different atmospheric environments (Wang et al., 2017; Kerminen et al., 2018; Nieminen et al., 2018; Chu et al., 2019; Bousiotis et al., 2021). Such characteristics describe mainly regional NPF, i.e. NPF averaged over relatively large spatial scales of at least tens of km. Much less information is available about local NPF, or about the small-scale variability of

51 regional NPF (Kulmala et al., 2024a, 2024b). Such information would be important in
52 identifying hot spot areas for atmospheric NPF or estimating the relative importance of
53 various local sources to regional NPF.
54
55 Atmospheric cluster ion (diameters below 2 nm) measurements can provide insight into ion
56 source processes, such as the ion production rate associated with different atmospheric
57 ionization pathways, as well as ion loss processes, such as ion-ion recombination or
58 scavenging of ions by a pre-existing atmospheric aerosol population (e.g. Hirsikko et al.,
59 2011; Kontkanen et al., 2013). Observations of intermediate ions (diameters between 2 and 7
60 nm) can be used to get information about atmospheric NPF (e.g. Tammet et al., 2014),
61 whereas small intermediate ions (approx. 2.0–2.3 nm) can be used to detect "local" NPF, i.e.
62 NPF taking place within a close proximity of a measurement site (Tuovinen et al., 2024).
63
64 Intermediate ions are sensitive to both occurrence and intensity of atmospheric NPF (e.g.
65 Horrak et al., 1998; Tammet et al., 2014, Leino et al., 2016). Recently, Kulmala et al. (2024a)
66 and Tuovinen et al. (2024) found that the smallest sizes of intermediate ions describe
67 relatively well the local production of new aerosol particles. These results were obtained
68 using a Neutral Cluster and Air Ion Spectrometer (NAIS; Mirme and Mirme, 2013). The
69 NAIS is, however, a sophisticated instrument that provides information not necessarily
70 needed when investigating local NPF, such as detailed knowledge of both ion and particle
71 number size distributions.
72
73 In this study, we will analyze data obtained using a Cluster Ion Counter (CIC; Mirme et al.,
74 2024), a recently developed and simple 3-channel instrument, and will investigate how this
75 instrument can be utilized to determine several variables important to NPF and small ion
76 dynamics. Our main objectives are to derive simple equations for characterizing ion
77 dynamics related to local NPF, and to find out whether the CIC is sensitive and reliable
78 enough for such purposes. In order to reach these objectives, we will first derive equations
79 that can be used to estimate condensation sink (CS), growth rate of newly formed particles
80 and formation rate of 2 nm ions, quantifying the intensity of local new particle formation
81 (actually local intermediate ion formation, LIIF), based on CIC measurements. Next, we will
82 compare ion concentrations between the CIC and NAIS, as measured at the SMEAR II
83 station in Hyytiälä, Finland. Finally, we will demonstrate how to apply CIC measurements in
84 practice for obtaining information about local NPF and related quantities, including the
85 condensation sink.
86
87 **2. Material and Methods**
88
89 **2.1 Cluster Ion Counter (CIC)**
90
91
92 The Cluster Ion Counter (CIC) is an instrument for measuring the total number concentration
93 of both positive and negative cluster ions. The CIC uses two separate first-order cylindrical
94 differential mobility analyzers, one for each polarity (Tammet, 1970). The principal
95 components of the analyzers are a central electrode on the axis of the analyzer that is held at a
96 steady voltage, and three cylindrical collecting electrodes flush with the outer wall of the
97 analyzer which are at zero electric potential. A constant sample flow is produced through the
98 analyzer using a blower at the outlet. The sampled ions passing through the analyzers are
99 repelled by the central electrode and they may deposit on one of the collecting electrodes
100 depending on the electrical mobility of the ions. The electric current produced by the

deposited ions is measured using high precision integrating electrometers (Mirme et al., 2024).

The mobility dependent detection efficiency curves of the three channels are determined by the geometry of the analyzer, sample air flow rate and the electric voltage of the central electrode. According to the idealized model of differential mobility analyzers (Tammet, 1970), the primary parameters governing the detection efficiency curves and the limiting mobilities of the collecting electrodes are the electrical capacitances between the central electrode and the each collecting electrode, as well as the ratio of sample flow rate to central electrode voltage. The original CIC was designed to allow the estimation of average cluster ion mobility. However, the device can easily be modified to focus on other aspects of the mobility distribution.

In the CIC, the flow rate-to-voltage ratio can be freely adjusted through software. The lengths of the collecting electrodes and geometry of the central electrode of the CIC can be changed without requiring additional modifications to the device.

A modified analyzer for the CIC was developed to estimate the concentration of intermediate ions roughly between 2.0 and 2.3 nm. Due to the relatively simple construction of the CIC, and specifically the absence of a separate sheath air flow layer in the mobility analyzer, the detection efficiency curves of the individual electrodes of the CIC are relatively wide and extend far towards larger particles (Figure 1). However it is notable that for particles beyond certain size the transfer functions differ only by a constant coefficient. We can use the signal from one channel to compensate for the concentration of larger particles in another channel and virtually achieve a higher size resolution.

We altered the collecting and central electrode geometry, as well as voltage, and flow rate within the mechanical constraints of the original device so that the transfer functions of channel 2 and 3 would differ only in a relative narrow size range and the difference would peak between 2.0 and 2.3 nm. This required extending the first collecting electrode and shortening the second and third electrode, as well as changing the diameter and length of the central electrode.

In the modified CIC, the signal from the first electrometer can be used to estimate the cluster ion concentrations. By subtracting the signal of the third channel from the signal of the second channel, the concentration of intermediate ions roughly between 2.0 and 2.3 nm can be estimated, denoted by Channel 2-3 from now on. The third channel can be utilized for ions from 2.3 to 5 nm.

2.2 Theoretical framework

The time evolution of sub-2 nm ion concentration, I, can be written as

$$\frac{dI}{dt} = Q - \alpha I^2 - \text{CoagS}_I \times I, \qquad\qquad (1)$$

where Q is the ion source rate, α ($\approx 1.6 \times 10^{-6}$ cm^3 s^{-1}; Franchin et al., 2015) is the ion-ion recombination rate, and CoagS_I is the coagulation sink of the sub-2 nm ions onto pre-existing aerosol particles. Other losses, such as deposition are assumed to be negligible. In a pseudo-steady state, we may approximate the left-hand side of eq.1 equal to zero, from which we obtain:

151
$$\text{CoagS}_I = Q/I - \alpha I. \tag{2}$$
153
154 The coagulation sink of neutral particles of diameter d_p can be connected with the
155 condensation sink (CS) of sulphuric acid monomers via (see Lehtinen et al., 2007)
156
$$\text{CS} \approx \text{CoagS}(d_p) \, (d_p/0.7 \text{ nm})^m , \tag{3}$$
158
159 where the exponent m depends on the shape of the pre-existing particle number size
160 distribution, and the diameter of a sulphuric acid monomer is estimated to be 0.7 nm. By
161 combining eqs. 2 and 3 we then obtain:
162
$$\text{CS} \approx \text{CoagS}(d_p = d_{p,I}) \times [d_p/0.7 \text{ nm}]^m \times [Q/I - \alpha I] / \text{CoagS}_I , \tag{4}$$
164
165 where $d_{p,I}$ refers to the median diameter of the sub-2 nm ions. In order to simplify eq. 4, we
166 will make three further approximations: 1) $d_{p,I}$ is equal to 1.2 nm for negative cluster ions
167 observed with CIC, and 1.0 nm for negative cluster ions measured with NAIS, 2) the
168 exponent m is equal to 1.6 (see Lehtinen et al., 2007), and 3) the ratio $\text{CoagS}(d_p = d_{p,I})$ /
169 CoagS_I is equal to 0.5 (Leppä et al., 2011; Mahfourz and Donahue, 2021). The $d_{p,I}$ were
170 determined as weighted mean diameters of 0.8-2.0 nm (NAIS) and 1.0-2.0 nm (CIC) negative
171 ions based on the NAIS ion number size distributions. The concentrations of ions in different
172 size bins were used as weights. By combining these approximations, we finally obtain:
173
$$\text{CS} \approx 1.2 \, (Q/I - \alpha I). \tag{5a}$$
175
$$\text{CS} \approx 0.9 \, (Q/I - \alpha I). \tag{5b}$$
177
178 Here we utilize eq. 5a if I is measured with the CIC and eq. 5b if I is measured with the
179 NAIS.
180
181 Similar to eq. 1, the time evolution of the concentration of the smallest (2.0–2.3 nm)
182 intermediate ions, N, can be written as
183
$$\frac{dN}{dt} = J_2 - \text{CoagS}_N \times N - J_{out}, \tag{6}$$
185
186 where J_2 is the formation rate of 2 nm ions, CoagS_N is the coagulation sink of the 2.0–2.3 nm
187 ions onto the pre-existing aerosol population, and J_{out} is the rate at which these ions grow out
188 of the 2.0–2.3 nm size range. CoagS_N and J_{out} can be approximated as:
189
$$\text{CoagS}_N \approx \text{CoagS}_I \times (1.2 \text{ nm} /2.1 \text{ nm})^{1.6} \approx 0.4 \, \text{CoagS}_I \approx 0.4 \, (Q/I - \alpha I), \tag{7}$$
191
$$J_{out} \approx \text{GR}_{2.3 \text{ nm}} \times N/\Delta \text{d}, \tag{8}$$
193
194 where $\text{GR}_{2.3 \text{ nm}}$ is the growth rate of 2.3 nm ions and Δd (=0.3 nm) is the width of the
195 intermediate ion channel of the CIC. Assuming a pseudo-steady state ($dN/dt = 0$) and using
196 Eqs. 2, 7 and 8, we then obtain:
197
$$J_2 = 0.4 \, (Q/I - \alpha I) \times N + \text{GR}_{2.3 \text{ nm}} \times N/\Delta d + \alpha IN. \tag{9}$$
199

200 The last term in Eq. 9 accounts for the loss rate of 2.0-2.3 nm ions due to their recombination
201 with sub-2 nm ions.
202
203 Particle (or ion) growth rates can be determined from the following equation:
204
205 $$GR = \frac{\Delta d_i}{\Delta t},$$ (10)
206
207 where Δd_i is the change of the diameter of ions over the time interval Δt as the ions grow in
208 size. In section 3.2 we will demonstrate how the CIC measurement can be used for
209 determining growth rates.
210
211 **2.3. Observations and data**
212
213 The CIC and NAIS were compared with each other at the SMEAR II station in Hyytiälä (Hari
214 and Kulmala, 2005) during 16 January–01 April, 2024; however, NAIS data were missing
215 from the period 16-17 March. The NAIS (Neutral Cluster and Air Ion Spectrometer) is a
216 multichannel instrument to measure atmospheric ions from 0.8 to 42 nm and total particle
217 concentrations from 2.5 to 42 nm (Mirme and Mirme, 2013). From NAIS, concentrations of
218 total sub-2 nm ions, 1-2 nm, and 2.0-2.3 nm were used in this study. In addition, as CIC
219 Channel 2-3 covers a slightly wider diameter range than 2-2.3 nm, we determined
220 concentrations corresponding to those within the same mobility diameter range from the ion
221 number size distributions measured by NAIS (NAIS Channel 2-3). The NAIS ion number
222 size distributions were multiplied by the detection efficiencies for the CIC Channel 2–3
223 (Figure 1), and then summed. The resulting total concentrations were assumed to correspond
224 to the detected ion concentration by CIC Channel 2-3. This concentration was then divided
225 by the average detection efficiency for the CIC Channel 2-3 to get the atmospheric ion
226 concentration. If the NAIS concentrations are assumed to be equal to the atmospheric
227 concentrations, then in theory the CIC and NAIS Channel 2-3 concentrations should be equal.
228 For convenience, CIC Channel 2-3, NAIS 2.0-2.3 nm, and NAIS Channel 2-3 are collectively
229 referred to as 2.0-2.3 nm ions when separating them is not necessary.
230
231 Furthermore, the conceptual model (see chapter 2.2) was used to analyse the data from both
232 SMEAR II and AHL/BUCT station in Beijing, China (Liu et al., 2020). In data analysis we
233 use 10%, 25%, 50%, 75%, and 90% percentiles for small and intermediate ion
234 concentrations and CS values. A longer time spans were used for this part of the analysis. For
235 Hyytiälä, the data cover most of the time between the beginning of 2016 and end of 2020. For
236 Beijing, ion concentrations were determined over the period 13 January 2018 to 01 April
237 2020, whereas the CS data cover the period 20 February 2018 to 31 March 2019. The particle
238 number size distributions to derive the CS data were measured by a twin DMPS (Differential
239 Mobility Particle Sizer; Aalto et al., 2001) in Hyytiälä and in Beijing by a particle size
240 distribution (PSD) system (Liu et al., 2016). See Zhou et al. (2020) for more details on the
241 measurements in Beijing.
242
243
244 **3. Results and Discussion**
245
246 **3.1 Instrument comparison**
247
248 In order to find out how reliably the CIC is able to observe ion concentrations, we compared
249 it with the NAIS at the SMEAR II station in Hyytiälä, Finland. Tables 1 and 2 summarize the

250 percentiles of the ion concentrations measured by these two instruments for different size
251 fractions. We can see that the total concentration of sub-2 nm negative ions measured by the
252 NAIS is significantly higher than those measured by the CIC (channel 1), the median
253 concentrations being equal to 530 and 210 cm^{-3}, respectively. This result is expected, as the
254 detection efficiency of both instruments decreases rapidly for particles smaller than 1 nm.
255 However, the NAIS is able to correct for this in data inversion, while the CIC is not due to
256 the lack of detailed information about the measured size distribution. Excluding the smallest
257 ions measured by the NAIS, i.e. considering only the 1–2 nm size range, the median
258 concentration drops down to 180 cm^{-3}. This is slightly below the median sub-2 nm
259 concentration measured by the CIC, but only about one third of the median total sub-2 nm ion
260 concentration measured by the NAIS.
261
262 A comparison between the two instruments is in Figure 2 for small (1-2 nm) ions, and in
263 Figure 3 for the smallest size class of intermediate ions (2.0–2.3 nm). We can see that when
264 the small ion concentration is above 200 cm^{-3}, the two instruments show similar values, while
265 at lower concentrations there is more spread in the values with the CIC generally measuring
266 higher concentrations than the NAIS. At low concentrations, it is possible that the
267 uncertainties in the detection efficiencies of the ions with diameters close to 1 nm impact the
268 results, explaining our observations. CIC Channel 2-3 concentration are consistently lower
269 than NAIS Channel 2-3 concentrations, with the difference being smaller when the
270 concentrations are higher, suggesting that a lower concentrations electronic noise impacts the
271 comparison increasingly. There is more spread between the values of NAIS 2.0-2.3 nm and
272 CIC Channel 2-3. At higher concentrations the CIC shows higher concentrations than NAIS
273 2.0-2.3 nm concentration. However, the overall the overall agreement between these two
274 instruments is good with the correlation coefficients of 0.85 and 0.86 for small ions and 2.0-
275 2.3 nm ions, respectively.
276
277 Figure 4 presents the time series of ion concentrations measured by the CIC and NAIS over
278 the whole two and half-month period, while Figure 5 presents the diurnal pattern of ion
279 concentrations on a selected day (10th of March, 2024). Total sub-2 nm ion concentrations
280 measured by the NAIS are higher than CIC Channel 1 ion concentrations. However, for
281 majority of the time (see Figure 4), the NAIS 1-2 nm ion concentration and CIC Channel 1
282 concentration are close to each other. On the selected day, CIC Channel 2-3 peak NAIS
283 Channel 2-3 values are similar, 60 and 80 cm^{-3}, respectively, whereas the NAIS 2.0-2.3 nm
284 peak value is lower at around 20 cm^{-3}. CIC Channel 2-3 is likely influenced by ions larger
285 than 2.3 nm, impacting the measured concentration when intermediate ion concentration is
286 high, such as during NPF. The correlation coefficient between the concentrations from the
287 two instruments on the selected day is around 0.9 for both sub-2 nm and 2.0-2.3 nm ions.
288
289 Comparing the lower percentiles in Tables 1 and 2, it is apparent that a large fraction of CIC
290 Channel 2-3 concentrations are negative. At very low concentrations (< 1 cm^{-3}), the signal is
291 mainly noise. In addition, Figure 4 and 5 show that the low background concentrations
292 measured by CIC Channel 2-3 are on average less than 10% of NAIS Channel 2-3
293 concentrations, which we postulate is due to estimation errors caused by the limited size
294 resolution of the NAIS as well as different background noise levels of the instruments . At
295 very low concentrations, the values from either instrument can be considered unreliable.
296 Regardless, within the scope of this study, these background concentrations are of less
297 interest compared to the higher concentrations. Periods of LIIF can be identified based on
298 elevated 2.0-2.3 nm ion concentrations, and these ion concentrations can then be used to
299 derive parameters, such as the ion formation rate, to quantify the intensity of LIIF. The

300 comparison of the two instruments done here has shown that we can use CIC measurements
301 to identify LIIF.
302
303 **3.2 Application of CIC measurement in investigating condensation sink and local NPF**
304
305 Figure 6 illustrates how the estimated condensation sink (CS) based on Eq. 5b behaves as a
306 function of small ion concentrations, I, for different ion production rates. In the same plot, we
307 have included the observed variability of CS as determined from the particle number size
308 distributions and I in both Hyytiälä and Beijing. We can see that measured and theoretically
309 calculated estimates of CS agree with each other the best when median ion production rates
310 are between about 2 and 4 ion pairs cm^{-3} s^{-1} in both Hyytiälä and Beijing.
311
312 The CIC has a higher detection efficiency for small ions than the NAIS due to a shorter inlet
313 tract, and consequently, lower inlet losses. However, in case of both instruments, the
314 detection efficiency for sub-2 nm ions is very strongly dependent on particle size. The NAIS
315 measures the size distribution of ions, and the data inversion algorithm uses that information
316 to correct for the size-dependent detection efficiency. The CIC has limited information about
317 the size distribution of detected ions, making it more difficult to correct for the detection
318 efficiency. Using the sub-2 nm ion concentrations from the NAIS and the CIC (Tables 1 and
319 2), we estimated how the concentrations measured using the CIC and NAIS will influence the
320 estimated values of CS. By using eq. 5 and by assuming the median sub-2 nm ion
321 concentrations measured by these two instruments (Tables 1 and 2), we may calculate that the
322 values of CS measured using the NAIS are 0.237, 0.256 and 0.266 times those measured
323 using the CIC for Q equal to 2,3 and 4, respectively. Therefore, if we use the CIC for
324 estimating CS via eq. 5a, the real CS (using NAIS and equation 5b) is about 0.25 times the
325 one observed by CIC.
326
327 Figure 7 shows the CS derived based on Eq. 5a and 5b versus CS determined from the full
328 particle number size distribution (CS_{DMPS}). We see that the CS predicted by NAIS varies less
329 than CS_{DMPS}, but is mostly within the same order of magnitude. CS predicted by CIC is
330 consistently higher than CS_{DMPS}. However, considering the above discussion, and multiplying
331 the estimated CS by 0.25, we get values much closer to CS_{DMPS}. Assuming Q=2, the CS
332 values predicted by CIC are mainly within a factor of three from CS_{DMPS} values.
333
334 We have assumed that the only losses of ions are due to their coagulation with larger particles
335 and their recombination with oppositely charged ions. In reality, processes such as deposition
336 also affect the ion concentration. For example, Tammet et al. (2006) found that in Hyytiälä
337 deposition of ions to forest canopy impacts small ion concentrations. In addition, we have
338 assumed the ion source rate to be constant. In reality, it is expected to vary somewhat, for
339 example due to varying radon concentration (e.g., Hirsikko et al., 2007). Therefore, the
340 presented method of determining CS can only give a rough approximation for CS.
341
342 In order to illustrate how the CIC can be used to determine the ion growth rate (GR), we
343 selected one measurement day (Figure 8) and determined GR using the appearance time
344 method (e.g. Lehtipalo et al., 2014) and equation (10). Ion concentrations from the CIC
345 Channel 2-3 and Channel 3 from February 13th were used. The ion concentrations were
346 smoothed using a moving 1-hour median method to lessen the impact of noise. As we can see
347 from Figure 8, Channel 3 and Channel 2–3 concentrations on the selected day have a similar
348 shape between 10:00 and 16:00, and the shape of the Channel 3 roughly follows that of
349 Channel 2–3 with a time delay. Considering the shape and features of the two curves, and the

350 times at which the two concentrations reach a similar fraction of the maximum concentration
351 (appearance time method,), two time instances were identified visually. The appearance times
352 were chosen to correspond to times when the ion concentrations were around 20 % of the
353 maximum concentrations. From these approximate appearance times, a time delay was
354 calculated. Based on Figure 1, the diameters of 2.2 nm and 2.9 nm for Channel 2–3 and 3
355 were assumed, respectively. We note that on this particular example day, the curves follow
356 each other closely for a span of several hours, so that the value of GR is not very sensitive to
357 the identified appearance times, i.e., the chosen fraction of the maximum concentration
358 anywhere between 0.2 and 0.9 results in the same approximate GR. The resulting GR was
359 approximately 0.9 nm/h. This value is in the expected range, as the earlier long-term
360 measurements at the same site indicate typical growth rates between about 1 and 2 nm/h for
361 sub-3 nm ions (Hirsikko et al., 2005; Manninen et al., 2010). We should note, however, that it
362 is not possible to determine GRs for all measurement days using the procedure presented
363 here. This is because even if an increase in ion concentrations was observed, the signal might
364 be too noisy, making the determination of appearance times too unreliable. In addition, not all
365 days exhibited a clear delay between the two appearance times, making the determination of
366 growth rate impossible.
367
368
369 Using Eq. 9, we can estimate the formation rate of 2 nm ions, J_2. Figure 8 shows these
370 formation rates for Hyytiälä and Beijing. This formation rate can be given as a function of the
371 measured number concentrations of 2.0–2.3 nm intermediate ions, in addition to which J_2
372 depends on the growth rate, ion source rate, and ion loss rate, the latter of which was
373 estimated using the sub-2 nm ion concentrations according to Eq. 5b. J_2 also depends on the
374 concentration of sub-2 nm ions, which is determined by the ion loss rate and ion source rate
375 (Eq. 1). For Figure 9, the median sub-2 nm ion concentrations in Hyytiälä and in Beijing
376 were used in Eq. 9. The most probable values are 1–2 nm/h for the growth rate in Hyytiälä
377 (Figure 8, Hirsikko et al., 2005; Manninen et al., 2010), 1–3 nm/h for the growth rate in
378 Beijing (Deng et al., 2020), and 2–3 cm^{-3} s^{-1} for the ion source rate (Figure 6). However, also
379 higher values are given for comparison. Manninen et al. (2010) calculated a median value of
380 0.06 cm^{-3} s^{-1} for J_2 based on long-term measurements in Hyytiälä, which is at the higher end
381 of values estimated in Figure 9. Compared with Hyytiälä, we estimate a factor of 2–4 larger
382 values of J_2 for Beijing. If one wants to estimate the total 2 nm particle formation rate, in both
383 places, it is considerably larger than the formation rate of 2 nm ions, being of the order of one
384 magnitude in Hyytiälä (Manninen et al., 2010, Kulmala et al., 2013) and even larger in
385 Beijing (Deng et al., 2020). These results are fully consistent with the general finding that on
386 average, observed new particle formation rates are 1 to 3 orders of magnitude larger in
387 polluted urban environments compared with clean or moderately polluted environments
388 (Kerminen et al., 2018; Nieminen et al., 2018), whereas the average formation rates of 2 nm
389 ions are typically within a factor of 2–3 between different environments (Manninen et al.,
390 2010).
391
392 Figure 10 shows the estimated time evolution of the condensation sink and 2-nm ion
393 formation rate during one day. The estimated value of CS varies only little, less than a factor
394 of 1.5, whereas the ion formation rate varies by more than two orders of magnitude during the
395 day. We can clearly see that when the estimated CS is at its lowest at around midday, the ion
396 formation rate is at its highest.
397
398
399 **4. Conclusions and summary**

400
401 The recent progress on finding local NPF (e.g. Kulmala et al., 2024; Tuovinen et al., 2024)
402 has opened a question: are we able to utilize a simple ion counter to identify and quantify
403 LIIF in a proper way? According to our results presented above, the answer is: yes.
404
405 We have developed a modified version of the CIC to measure sub-2 nm ion and 2.0–2.3 nm
406 ion concentrations as accurately as possible (Mirme et al., 2024). From the former quantity
407 we get information on the dynamics of small ions, including an estimate of the coagulation
408 sink of ions and, via equations (2) and (5), also condensation sink. Furthermore, the CIC
409 makes it possible to estimate the growth rate from about 2 nm to 3 nm and, with this
410 information, the formation rate of 2 nm ions, which we can use to quantify the intensity of
411 LIIF. While we have focused on negative ions in this paper, the same principles are also valid
412 for positive ions. LIIF is more sensitive to negative ions (Tuovinen et al., 2024), and thus
413 negative ions were investigated.
414
415 We compared the CIC with the NAIS in Hyytiälä, which demonstrates that the measured ion
416 concentrations from CIC are able to capture the temporal behavior of the ions such as the
417 variation in concentrations due to LIIF. The comparison of the estimated condensation sink
418 from ion concentrations using the ion balance equation with the observed ones in Hyytiälä
419 and Beijing demonstrates how the CIC, together with the simple theoretical framework, can
420 be used to estimate condensation sink, coagulation sink of ions and the ion formation rate. In
421 addition, the comparison of estimated CS based on CIC measurements with the CS
422 determined particle number size distributions shows that we can get estimates that are within
423 a factor three of the real CS. . Therefore, we can conclude that the CIC is an effective
424 instrument to observe LIIF and CS. Since CIC is ca seven times cheaper and requires less
425 maintenance than NAIS, with CIC one can have more observation locations and have wider
426 data coverage than with NAIS. However, if we want to investigate aerosol formation and
427 growth rates for the nucleation mode (3–25 nm), as is usually the case in investigating
428 regional NPF, NAIS measurements are needed.
429

430 **Author contribution**
431

432 Markku Kulmala had the original idea after discussions with Heikki Junninen. SM and PK
433 developed the CIC. LA performed CIC and NAIS comparison in Hyytiälä. ST and MK
434 analyzed the data. VMK and MK derived the used equations. YL lead the observations in
435 Beijing and TP in Hyytiälä. HJ, VMK, TP and ST contributed to developing the idea further.
436 MK, VMK and ST wrote the first version of the paper. All coauthors contributed the final
437 version of the paper.
438

439 **Competing interests**
440

441 Markku Kulmala is a member of the editorial board of Aerosol Research. The authors have
442 no other competing interests to declare.
443

References

Aalto, P., Hämeri, K., Becker, E., Weber, R., Salm, J., Mäkelä, J. M., Hoell, C., O'dowd, C. D., Hansson, H.-C., Väkevä, M., Koponen, I. K., Buzorius, G., and Kulmala, M.: Physical characterization of aerosol particles during nucleation events, Tellus B, 53, 344–358, doi:10.1034/j.1600-0889.2001.530403.x, 2001.

Boucher, O., Randall, D., Artaxo, P., Bretherton, C., Feingold, G., Forster, P., Kerminen, V.-M., Kondo, Y., Liao, H., Lohmann, U., Rasch, P., Satheesh, S., Sherwood, S., Stevens, B., and Zhan, X.: Clouds and Aerosols, in: Climate Change 2013: The Physical Science Basis. Contribution of Working Group I to the Fifth Assessment Report of the Intergovernmental Panel on Climate Change, edited by: Stocker, T., Qin, D., Plattner, G., Tignor, M., Allen, S., Boschung, J., Nauels, A., Xia, Y., Bex, V., and Midgley, P., Cambridge University Press, Cambridge, United Kingdom and New York, NY, USA, 2013.

Bousiotis, D., Pope, F. D., Beddows, D. C. S., Dall'Osto, M., Massling, A., Nøjgaard, J. K., Nordstrøm, C., Niemi, J. V., Portin, H., Petäjä, T., Perez, N., Alastuey, A., Querol, X., Kouvarakis, G., Mihalopoulos, N., Vratolis, S., Eleftheriadis, K., Wiedensohler, A., Weinhold, K., Merkel, M., Tuch, T., and Harrison, R. M.: A phenomenology of new particle formation (NPF) at 13 European sites, Atmos. Chem. Phys., 21, 11905–11925, https://doi.org/10.5194/acp-21-11905-2021, 2021.

Chu, B., Kerminen, V.-M., Bianchi, F., Yan, C., Petäjä, T., and Kulmala, M.: Atmospheric new particle formation in China, Atmos. Chem. Phys., 19, 115-138, https://doi.org/10.5194/acp-19-115-2019, 2019.

Deng, C., Fu, Y., Dada, L., Yan, C., Cai, R., Yang, D., Zhou, Y., Yin, R., Lu, Y., Li, X., Qiao, X., Fan, X., Nie, W., Kontkanen, J., Kangasluoma, J., Chu, B., Ding, A., Kerminen, V.-M., Paasonen, P., Worsnop, D. R., Bianchi, F., Liu, Y., Zheng ,J., Wang, L., Kulmala, M., and Jiang, J.: Seasonal characteristics of new particle formation and growth in Urban Beijing, Environ. Sci. Technol., 54, 8547-8557, 2020.

Franchin, A., Ehrbart, S., Leppä, J., Nieminen, T., Gagne, S., Schobesberger, S., Wimmer, D., Duplissy, J., Riccobono, F., Dunne, E. M., Rondo, L., Downard, A., Bianchi, F., Kupc, A., Tsagkogeorgas, G., Lehtipalo, K., Manninen, H. E., Almeida, J., Amorim, A., Wagner, P. E., Hansel, A., Kirkby, J., Kurten, A., Donahue, N. M., Makhmutov, V., Mathot, S., Metzger, A., Petäjä, T., Schnitzhofer, R., Sipilä, M., Stozhkov, Y., Tome, A., Kerminen, V.-M., Carslaw, K.,

Curtius, J., Baltensperger, U., and Kulmala, M.: Experimental investigation of ion-ion recombination under atmospheric conditions, Atmos. Chem. Phys., 15, 7203-7216, 2015.

Gordon, H., Kirkby, J., Baltensperger, U., Bianchi, F., Breitenlechner, M., Curtius, J., Dias, A., Dommen, J., Donahue, N. M., Dunne, E. M., Duplissy, J., Ehrhart, S., Flagan, R. C., Frege, C., Fuchs, C., Hansel, A., Hoyle, C. R., Kulmala, M., Kürten, A., Lehtipalo, K., Makhmutov, V., Molteni, U., Rissanen, M. P., Stozhov, Y., Tröstl, J., Tsakogeorgas, G., Wagner, R., Williamson, C., Wimmer, D., Winkler, P. M., Yan, C., and Carslaw, K. S.: Causes and importance of new particle formation in the present-day and preindustrial atmospheres. J. Geophys. Res. Atmos., 122, 8739-8760, https://doi.org/10.1002/2017JD026844, 2017.

Guo, S., Hu, M., Zamora, M. L., Peng, J., Shang, D., Zheng, J., Du, Z., Wu, Z., Shao, M., Zeng, L., Molina, M. J., and Zhang, R.: Elucidating severe urban haze formation in China, Proc. Natl. Acad. Sci. U.S.A., 111, 17373, https://doi.org/10.1073/pnas.1419604111, 2014.

Hari, P. and Kulmala, M.: Station for measuring Ecosystem-Atmosphere relations (SMEAR II), Boreal Environment Research, 10, 2005.

Hirsikko, A., Laakso, L., Hõrrak, U., Aalto, P. P., Kerminen, V.-M., and Kulmala, M.: Annual and size dependent variation of growth rates and ion concentrations in boreal forest, Boreal Env. Res., 10, 357-369, 2005.

Hirsikko, A., Paatero, J., Hatakka, J., and Kulmala, M.: The ^{222}Rn activity concentration, external radiation dose and air ion production rates in a boreal forest in Finland between March 2000 and June 2006, Boreal Environ. Res., 12, 265–278, 2007.

Hirsikko, A., Nieminen, T., Gagne, S., Lehtipalo, K., Manninen, H. E., Ehn, M., Horrak, U., Kerminen, V.-M., Laakso, L., McMurry, P. H., Mirme, A., Mirme, S., Petäjä, T., Tammet, H., Vakkari, V., Vana, M., and Kulmala, M.: Atmospheric ions and nucleation: a review of observations, Atmos. Chem. Phys., 11, 767-798, 2011.

Horrak, U., Salm, J., and Tammet, H.: Bursts of intermediate ions in atmospheric air, J. Geophys. Res.-Atmos., 103(D12), 13909–13915, 1998.

Kerminen, V.-M., Chen, X., Vakkari, V., Petäjä, T., Kulmala, M., and Bianchi, F.: Atmospheric new particle formation and growth: review of field observations, Environ. Res. Lett., 13, 103003, DOI 10.1088/1748-9326/aadf3c, 2018.

Kontkanen, J., Lehtinen, K. E. J., Nieminen, T., Manninen, H. E., Lehtipalo, K., Kerminen, V.-M., and Kulmala, M.: Estimating the contribution of ion-ion recombination to sub-2 nm cluster concentrations from atmospheric measurements, Atmos. Chem. Phys., 13, 11391-11401, 2013.

Kulmala, M., Kontkanen, J., Junninen, H., Lehtipalo, K., Manninen, H. E., Nieminen, T., Petäjä, T., Sipilä, M., Schobesberger, S., Rantala, P., Franchin, A., Jokinen, T., Järvinen, E., Äijälä, M., Kangasluoma, J., Hakala, J., Aalto, P. P., Paasonen, P., Mikkilä, J., Vanhanen, J., Aalto, J., Hakola, H., Makkonen, U., Ruuskanen, T., Mauldin, R. L., Duplissy, J., Vehkamäki, H., Bäck, J., Kortelainen, A., Riipinen, I., Kurtén, T., Johnston, M. V., Smith, J. N., Ehn, M., Mentel, T. F., Lehtinen, K. E. J., Laaksonen, A., Kerminen, V.-M., and Worsnop, D. R.: Direct observations of atmospheric aerosol nucleation, Science, 339, 943–946, https://doi.org/10.1126/science.1227385, 2013.

Kulmala, M., Cai, R., Stolzenburg, D., Zhou, Y., Dada, L., Guo, Y., Yan, C., Petäjä, T., Jiang, J., and Kerminen, V.-M.: The contribution of new particle formation and subsequent growth to haze formation, Environ. Sci.: Atmos., 2, 352-361, 2022

Kulmala, M., Ke, P., Lintunen, A., Peräkylä, O., Lohtander, A., Tuovinen, S., Lampilahti, J., Kolari, P., Schiestl-Aalto, P., Kokkonen, T., Nieminen, T., Dada, L., Ylivinkka, I., Petäjä, T., Bäck, J., Lohila, A., Heimsch, L., Ezhova, E., and Kerminen, V.-M.: A novel concept for assessing the potential of different boreal ecosystems to mitigate climate change (CarbonSink+ Potential). Boreal Env. Res., 29, 1–16, 2024a.

Kulmala, M., Aliaga, D., Tuovinen, S., Cai, R., Junninen, H., Yan, C., Bianchi, F., Cheng, Y., Ding, A., Worsnop, D. R., Petäjä, T., Lehtipalo, K., Paasonen, P., and Kerminen, V.-M. (2024) Opinion: A paradigm shift in investigating the general characteristics of atmospheric new particle formation using field observations, Aerosol Res., 2, 49-58, https://doi.org/10.5194/ar-2-49-2024, 2024b.

Lehtinen, K. E. J., Dal Maso, M., Kulmala, M., and Kerminen V.-M.: Estimating nucleation rates from apparent particle formation rates and vice-versa: Revised formulation of the Kerminen-Kulmala equation, J. Aerosol Sci., 38, 988-994, 2007.

Lehtipalo, K., Leppä, J., Kontkanen, J., Kangasluoma, J., Franchin, A., Wimmer, D., Schobesberger, S., Junninen, H., Petäjä, T., Sipilä, M., Mikkilä, J., Vanhanen, J., Worsnop, D. R., and Kulmala, M.: Methods for determining particle size distribution and growth rates between 1 and 3 nm using the Particle Size Magnifier, Boreal Environ. Res., 19, 215–236, 2014.

Leino, K., Nieminen, T., Manninen, H. E., Petäjä, T., Kerminen, V.-M., and Kulmala, M.: Intermediate ions as a strong indicator of new particle formation bursts in boreal forest, Boreal Env. Res., 21, 274-286, 2016.

Leppä, J., Anttila, T., Kerminen, V.-M., Kulmala, M., and Lehtinen, K. E. J.: Atmospheric new particle formation: real and apparent growth of neutral and charged particles, Atmos. Chem. Phys., 11, 4939-4955, 2011.

Liu, J. Q., Jiang, J. K., Zhang, Q., Deng, J. G., and Hao, J. M.: A spectrometer for measuring particle size distributions in the range of 3 nm to 10 μm, Front. Env. Sci. Eng., 10, 63–72, https://doi.org/10.1007/s11783-014-0754-x, 2016.

Liu Y., Yan C., Feng Z., Zheng F., Fan X., Zhng Y., Li C., Zhou Y, Lin Z., Guo Y., Zhang Y., Ma L., Zhou W., Liu Z., Dada L., Dällenback K., Kontkanen J., Cai R., Chan T., Chu B., Du W., Yao L., Wang Y., Cai J., Kangasluoma J., Kokkonen T., Kujansuu J., Rusanen A., Deng C., Fu Y., Yin R., Li X., Lu Y., Liu Y., Lian C., Yang D., Wang W., Ge M., Wang Y., Worsnop D. R., Junninen H., He H. Kerminen V.-M., Zheng J., Wang L., Jiang J., Petäjä T., Bianchi F. and Kulmala M. (2020) Continuous and comprehensive atmospheric observations in Beijing: a station to understand the complex urban atmospheric environment. *Big Earth Data* **4**, 295-321.

Mahfouz, N. G. A. and Donahue, N. M.: Technical note: The enhancenment limit of coagulation scavenging of small charged particles. Atmos. Chem. Phys., 21, 3827-3832, 2021.

Manninen, H. E., Nieminen, T., Asmi, E., Gagne, S., Häkkinen, S., Lehtipalo, K., Aalto, P., Vana, M., Mirme, A., Mirme, S., Hõrrak, U, Plass-Dülmer, C., Stange, G., Kiss, G., Hoffer, A., Töro, N., Moerman, M., Henzing, B., de Leeuw, G., Brinkenberg, M., Kouvarakis, G. N., Bougiatioti, A., Mihalopoulos, N., O'Dowd, C. D., Ceburnis, D., Arneth, A., Svenningsson, B., Swietlicki, E., Tarozzi, L., Decesari, S., Facchini, M. C., Birmili, W., Sonntag, A., Wiedensohler, A., Boulon, J., Sellegri, K., Laj, P., Gysel, M., Bukowiecki, N., Weingartner, E., Wehrle, G., Laaksonen, A., Hamed, A., Joutsensaari, J., Petäjä, T., Kerminen, V.-M., and Kulmala, M.: EUCAARI ion spectrometer measurements at 12 European sites – analysis of new particle formation events, Atmos. Chem. Phys., 10, 7907-7927, 2020.

Mirme, S. and Mirme, A.: The mathematical principles and design of the NAIS – a spectrometer for the measurement of cluster ion and nanometer aerosol size distributions, Atmos. Meas. Tech., 6, 1061–1071, doi:10.5194/amt-6-1061-2013, 2013.

Mirme, S., Balbaaki, R., Manninen, H.E., Koemets, P., Sommer, E., Rörup, B, Wu, Y., Almeida, J., Sebastian, E., Weber, S.K, Pfeifer, J., Kangasluoma. J., Kulmala, M., Kirkby, J. Design and performance of the Cluster Ion Counter (CIC), to be submitted to Atmos. Meas. Tech., 2024

Nieminen, T., Kerminen, V.-M., Petäjä, T., Aalto, P. P., Arshinov, M., Asmi, E., Baltensperger, U., Beddows, D. C. S., Beukes, J. P., Collins, D., Ding, A., Harrison, R. M., Henzing, B., Hooda, R., Hu, M., Hõrrak, U., Kivekäs, N., Komsaare, K., Krejci, R., Kristensson, A., Laakso, L., Laaksonen, A., Leaitch, W. R., Lihavainen, H., Mihalopoulos, N., Németh, Z., Nie, W., O'Dowd, C., Salma, I., Sellegri, K., Svenningsson, B., Swietlicki, E., Tunved, P., Ulevicius, V., Vakkari, V., Vana, M., Wiedensohler, A., Wu, Z., Virtanen, A., and Kulmala, M.: Global analysis of continental boundary layer new particle formation based on long-term measurements, Atmos. Chem. Phys., 18, 14737–14756, https://doi.org/10.5194/acp-18-14737-2018, 2018.

Tammet, H.: The aspiration method for the Determination of Atmospheric-Ion Spectra, The Israel Program for Scientific Translations Jerusalem, National Science Foundation, Washington, D.C., 1970.

Tammet, H., Hõrrak, U., Laakso, L., and Kulmala, M.: Factors of air ion balance in a coniferous forest according to measurements in Hyytiälä, Finland, Atmos. Chem. Phys., 6, 3377–3390, doi:10.5194/acp-6-3377-2006, 2006.

Tammet, H, Komsaare, K., and Horrak, U.: Intermediate ions in the atmosphere, Atmos. Res., 135-136, 263-273, https://doi.org/10.1016/j.atmosres.2012.09.009, 2014.

Tuovinen, S., Lampilahti, J., Kerminen, V.-M., and Kulmala, M.: Intermediate ions as indicator for local new particle formation, *Aerosol Res*., 2, 93-105, https://doi.org/10.5194/ar-2-93-2024, 2024.

Wang, Z., Wu, Z., Yue, D., Shang, D., Guo, S., Sun, J., Ding, A., Wang, L., Jiang, J., Guo, H., Gao, J., Cheung, H. C., Morawska, L., Keywood, M., and Hu, M.: New particle formation in China: Current knowledge and further directions, Sci. Total Environ., 577, 258-266, 2017.

Zhou, Y., Dada, L., Liu, Y., Fu, Y., Kangasluoma, J., Chan, T., Yan, C., Chu, B., Daellenbach, K. R., Bianchi, F., Kokkonen, T. V., Liu, Y., Kujansuu, J., Kerminen, V.-M., Petäjä, T., Wang, L., Jiang, J., and Kulmala, M.: Variation of size-segregated particle number concentrations in wintertime Beijing, Atmos. Chem. Phys., 20, 1201–1216, https://doi.org/10.5194/acp-20-1201-2020, 2020.

Tables

Table 1. Percentiles of the CIC Channel 1 (small ion) and Channel 2–3 (roughly 2.0–2.3 nm ion) concentrations (cm^{-3}) during 16.01.2024–01.04.2024. Positive polarity is marked by + and negative by –. The negative concentrations for the Channel 2 subtracted by Channel 3 are indicative of a noisy signal of the instrument.

	Channel 1		Channel 2 - 3	
	+	–	+	–
Mean	280	220	2.8	5.2
10%	130	90	−11	-13
25%	190	140	−4.4	-5.6
50%	270	210	1.3	0.9
75%	360	290	7.9	9.6
90%	430	380	17	24

Table 2. Percentiles of NAIS concentrations (cm^{-3}) during 16.01.2024 – 01.04.2024, excluding 16–17.03.2024. Small ions in the diameter ranges 0.8–2 nm and 1–2 nm are included. Intermediate ion concentrations are included for diameter range 2.0–2.3 nm, as well as for the diameter range that the CIC covers (Channel 2–3, see Sect. 2.3 for details). Positive polarity is marked by + and negative by –.

	0.8–2 nm		1–2 nm		2.0–2.3 nm		Channel 2–3	
	+	–	+	–	+	–	+	–
Mean	490	540	400	210	2.0	2.3	17	13
10%	360	400	270	95	0.2	0.04	8.7	2.8
25%	410	460	330	120	0.7	0.3	11	4.5
50%	490	530	400	180	1.5	1.1	14	7.5
75%	570	620	470	270	2.7	2.6	19	14
90%	640	700	540	380	4.2	4.8	29	26

15

479
480 **Figures**
481
482
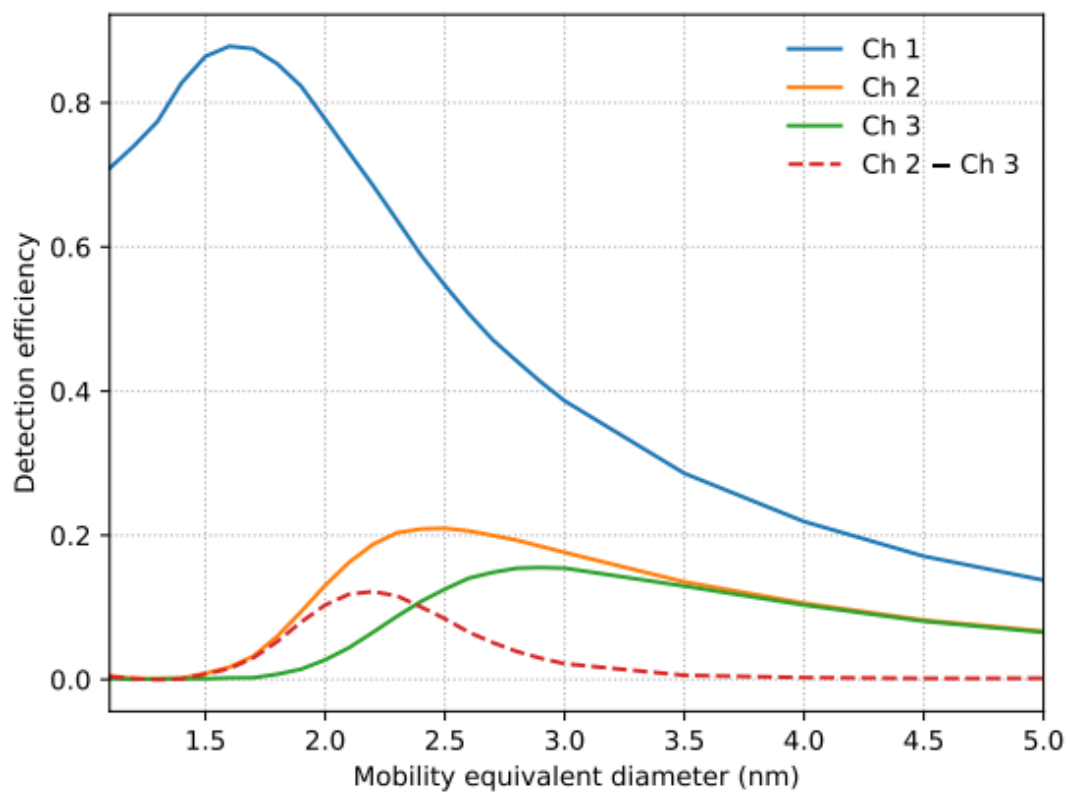
483
484
485
486 Figure 1. Experimental detection efficiency for ions in the range from 1.1 to 5.0 nm for each
487 of the 3 collecting electrodes of the CIC. Due to the absence of a separate sheath air flow
488 layer in the mobility analyzer, the detection efficiencies do not have a sharp upper size limit;
489 instead, they asymptotically approach zero as particle size increases. Ion concentrations in a
490 narrower size range can be estimated by subtracting the signal of channel 3 from channel
491 2. The detection efficiencies of the two channels converge from 2.5 nm to 3.5 nm and are
492 practically equal for larger particles.
493
494
495
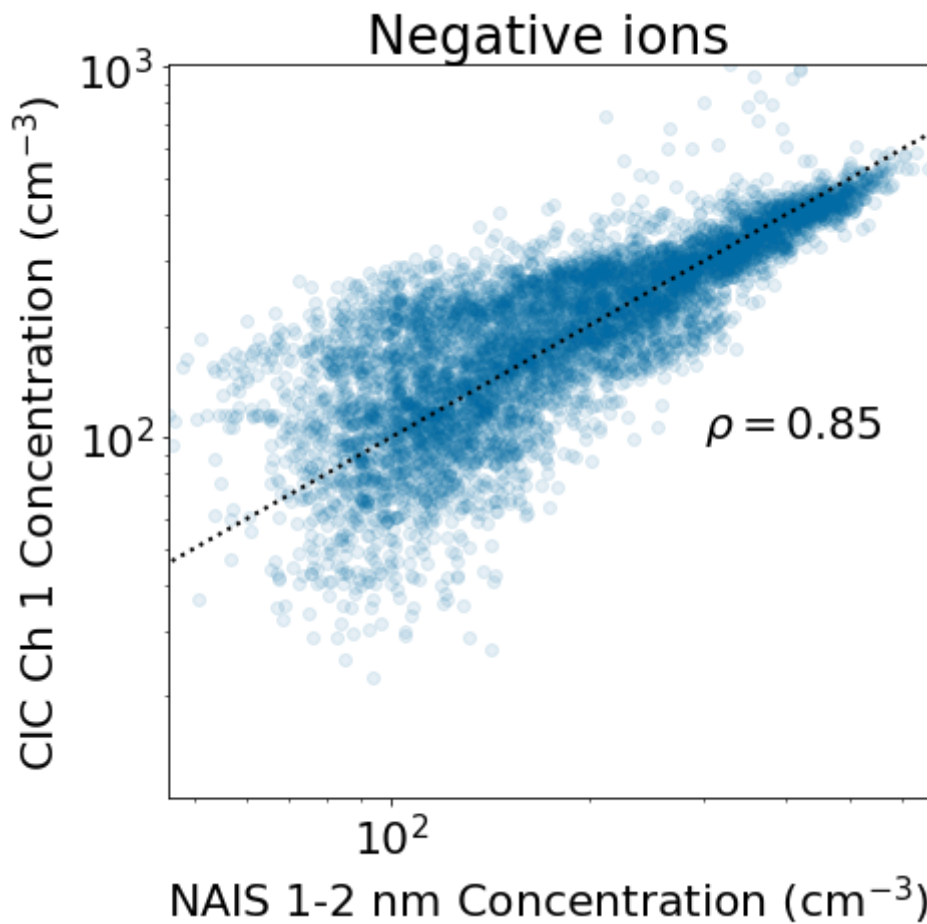
Figure 2. Scatter plot of the 15-min median negative small ion concentration measured with the CIC as a function of the concentration measured with the NAIS in Hyytiälä. The NAIS concentrations are from the diameter range 1–2 nm, while the CIC concentrations are from Channel 1. The black dotted line marks the 1:1 line. Pearson correlation coefficient ρ of the two concentrations shown is included in the figure.
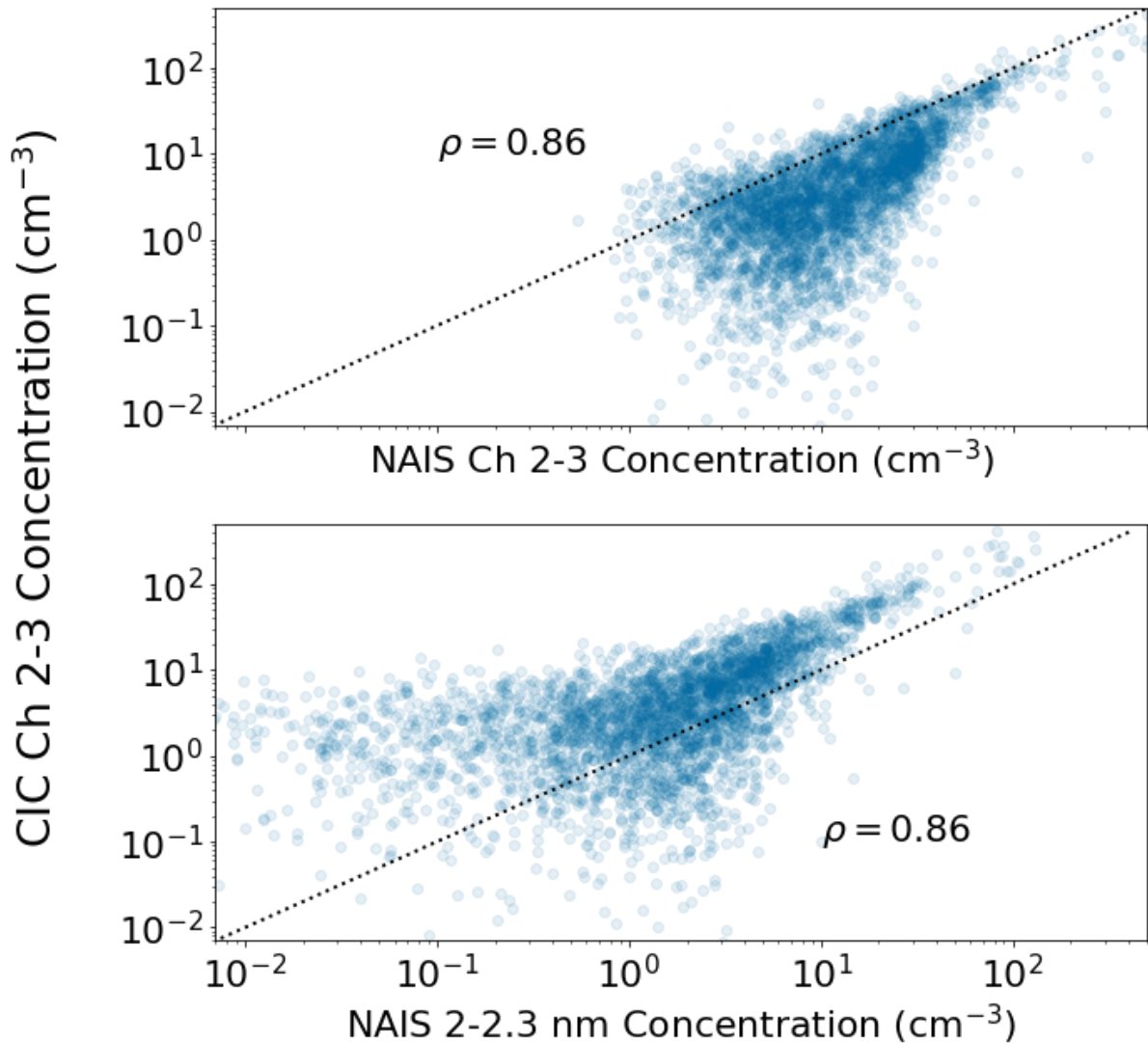
504
505 Figure 3. Scatter plot of approximately 2.0–2.3 nm negative ion 15-minute-median
506 concentrations measured with the CIC as a function of concentrations measured with the
507 NAIS in Hyytiälä. The NAIS concentrations on the top figure were determined for the same
508 size range as covered by the CIC Channels 2 and 3 (for details, see Sect. 2.3). The NAIS
509 concentrations on the bottom figure are for the diameter range 2.0–2.3 nm. The black dotted
510 line marks the 1:1 line. Pearson correlation coefficient ρ of the two concentrations shown is
511 included in the figure.
512
513
514

515
516 Figure 4. Time series of observed ion concentrations. The top figure has the concentrations of
517 small ions from the CIC Channel 1 and from the NAIS for both all sub-2 nm ions and 1–2 nm
518 ions. The bottom figure has concentrations of ions measured by the CIC channel 2–3 which
519 approximately corresponds to the size range of 2.0–2.3 nm. In addition, there are
520 concentrations of 2.0–2.3 nm ions measured by the NAIS (NAIS 2.0–2.3 nm) and
521 concentrations from the NAIS that were determined for the exact same size range as covered
522 by the difference of CIC Channels 2 and 3 (NAIS Ch 2-3).
523
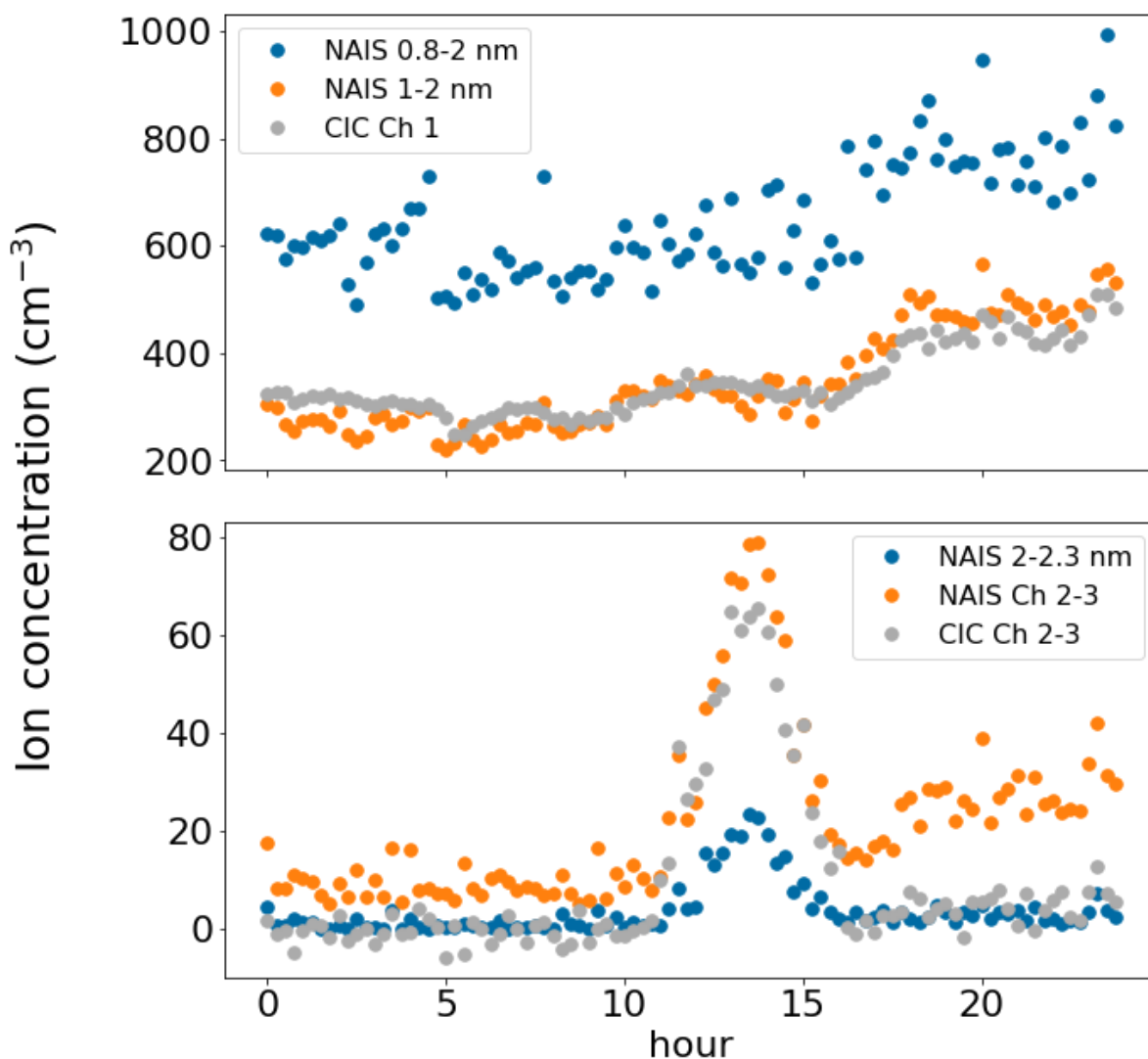
Figure 5. Observed negative ion concentrations on 10.03.2024. The top figure has the concentrations of small ions. For CIC, they are from the CIC Channel 1. From the NAIS, concentrations for all measured sub-2 nm ions and based on the size range 1–2 nm are included. The bottom figure has the concentrations of intermediate ions. For CIC, they are from Channel 2–3, corresponding to roughly 2.0–2.3 nm size range. For NAIS, the concentrations of ions between 2.0 and 2.3 nm are included, as well as the concentrations that were determined for the exact same size range as covered by the CIC Channels 2 and 3 (NAIS Ch 2–3). The correlation coefficients on this day are 0.83, 0.95, 0.93 and 0.90 for NAIS 0.8-2 nm vs CIC Channel 1, NAIS 1–2 nm vs CIC Channel 1, NAIS 2.0-2.3 vs CIC Channel 2–3, and NAIS Channel 2–3 vs CIC Channel 2–3, respectively.
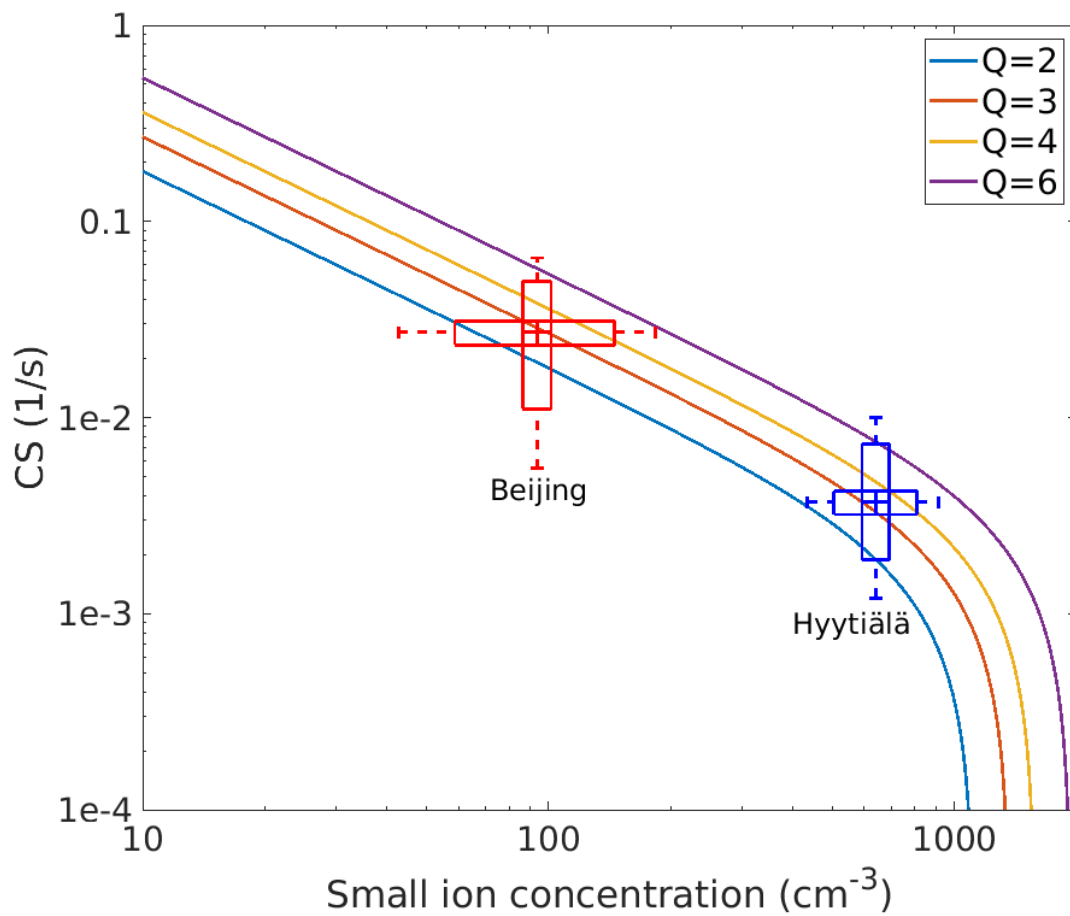
Figure 6. Condensation sink (CS) as function of the small ion concentration for different ion source rates (Q, ions cm^{-3} s^{-1}). The observed values of I and CS in Hyytiälä and Beijing (medians marked by the center line of the boxplot, 25% and 75% quartiles marked by the edges, and 10% and 90% percentiles marked by the whiskers of the boxplots) indicate ion source rates between about 2 and 4 cm^{-3} s^{-1} in both places.
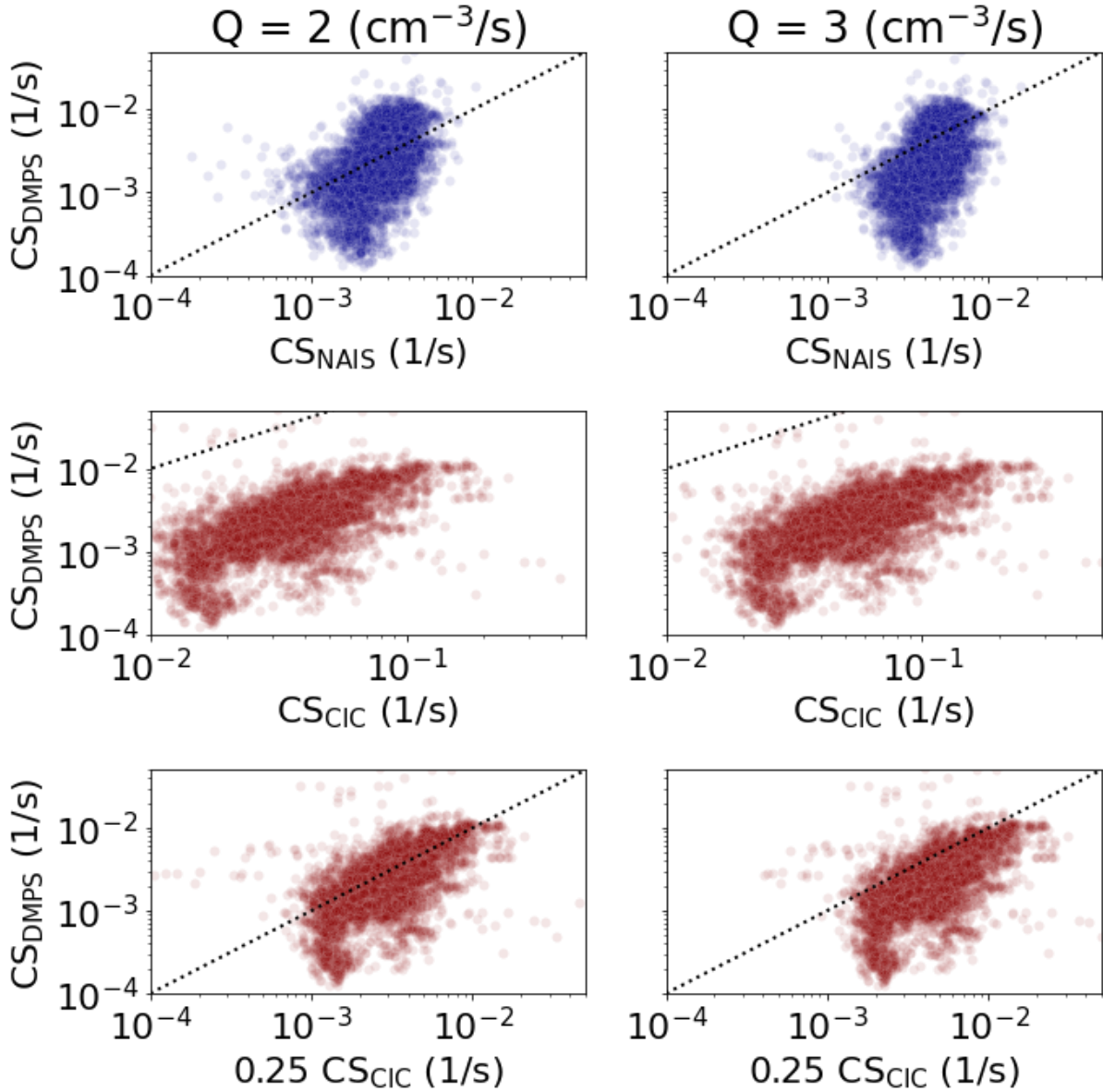
Figure 7: Condensation sink (CS) determined based on particle number size distribution data measured by DMPS versus CS derived based on negative sub-2 nm ion concentrations from NAIS and CIC. For CIC and NAIS, Eq. 5a and 5b have been used, respectively.
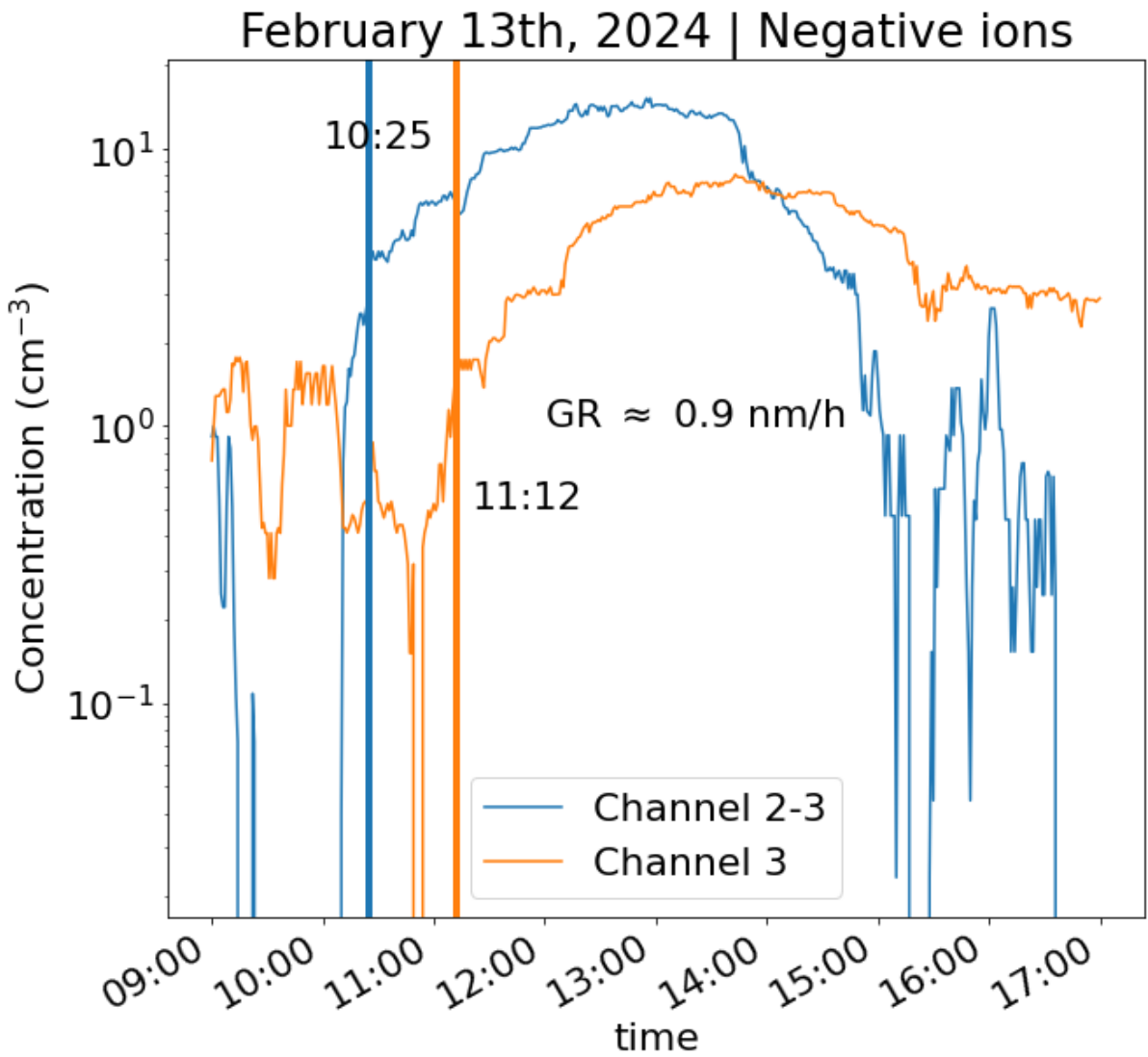
Figure 8: The CIC Channel 3 and Channel 2-3 concentrations on the day of February 19th.
Approximate appearance times have been marked by vertical lines alongside the growth rate
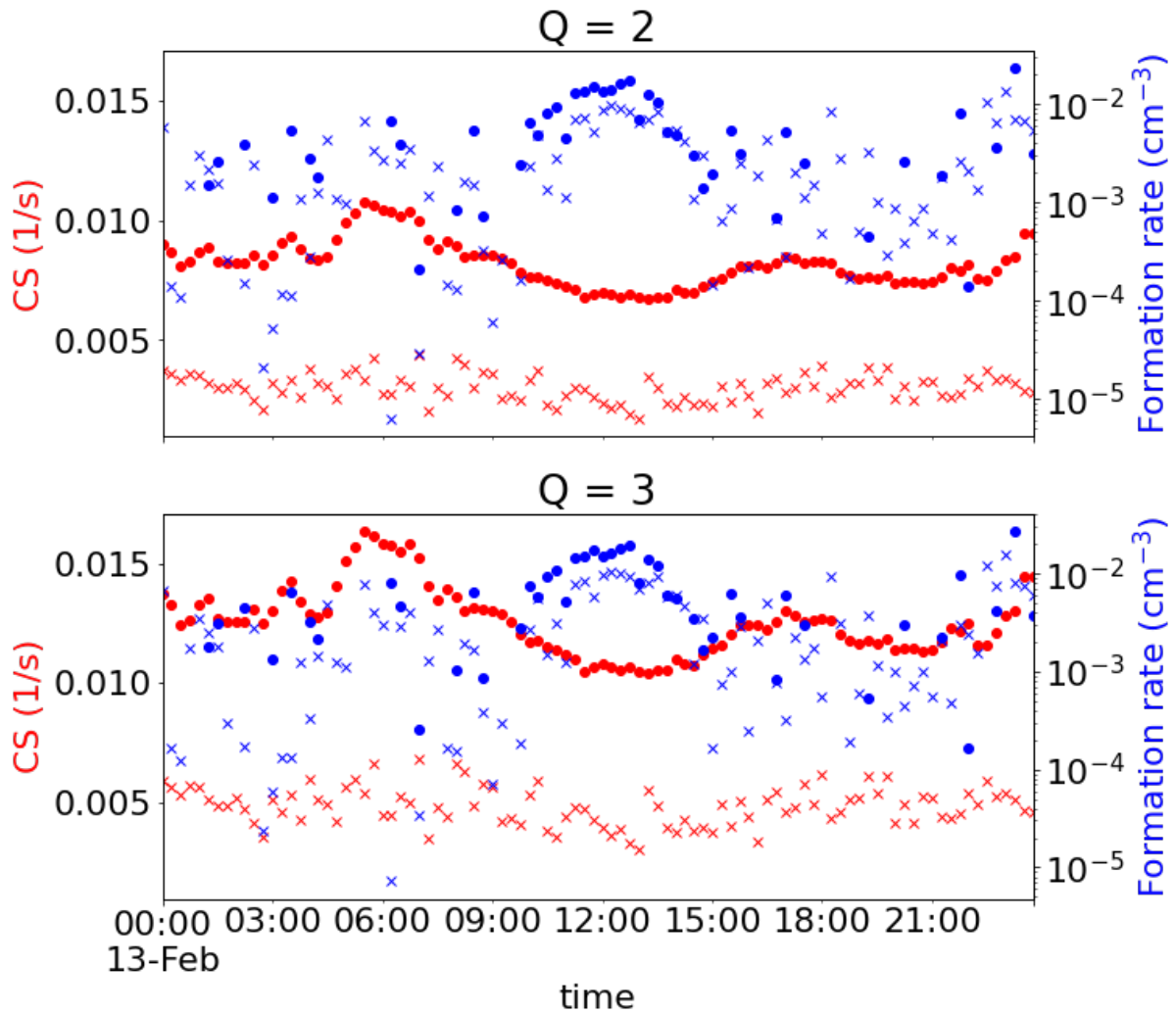(GR) from 2.2 to 2.9 nm derived based on those appearance times.
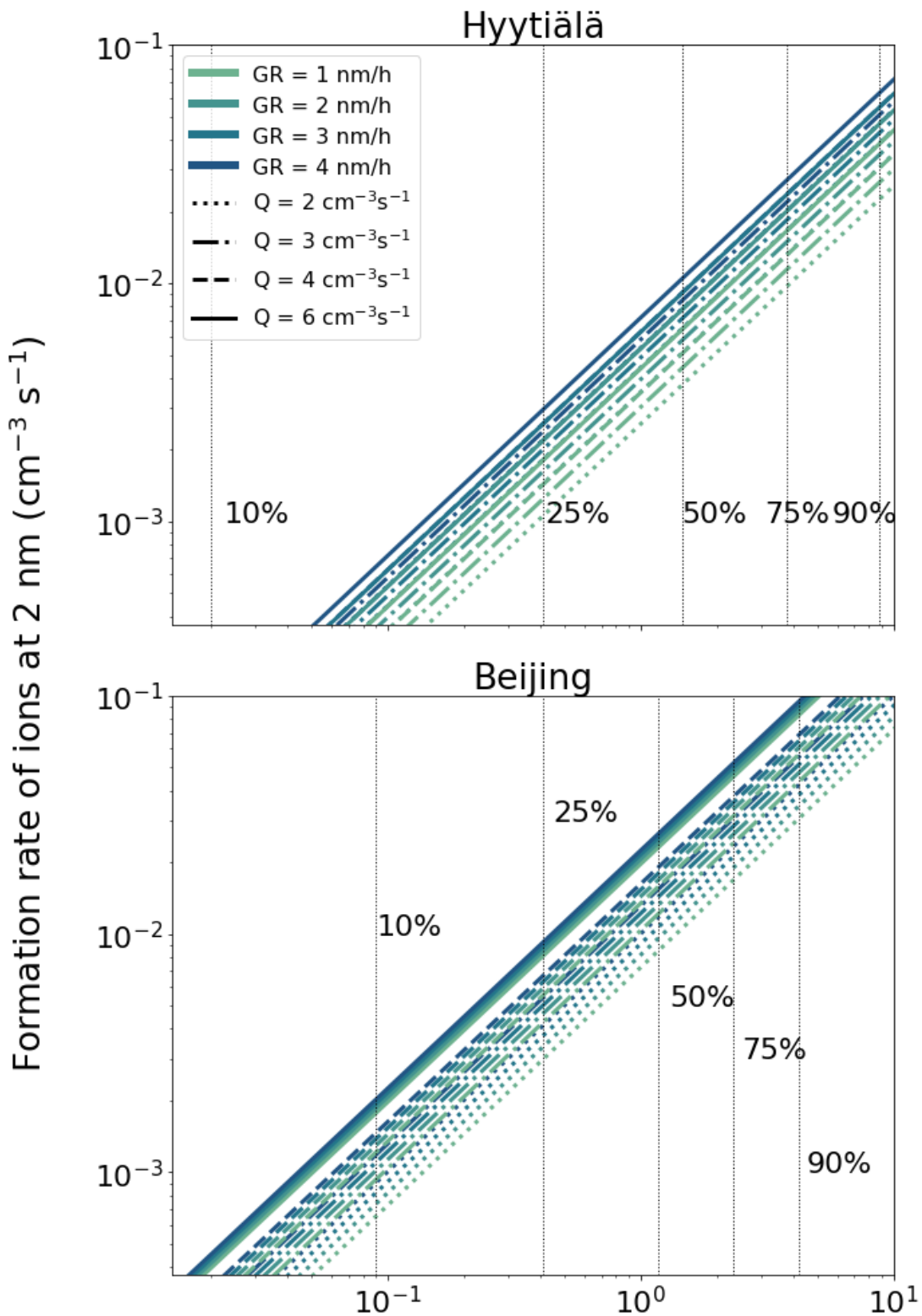
Figure 9: The estimated formation rate of 2 nm negative ions as a function of the concentration of 2.0-2.3 nm ions. The ion growth rate has been assumed to be equal to 1 nm/h.The 10%, 25%, 50%, 75, 90% concentration values are indicated by the vertical lines.

Figure 10: Condensation sink (right) and formation rate of 2 nm ions (left). The values marked by dots are based on CIC channel 1 and channel 2-3 ion negative ion concentrations while the values marked by x markers are based on NAIS sub-2 nm and 2.0-2.3 nm negative ion concentrations. The top panel has valued with assumed ion source rate of Q= 2 cm^{-3} s^{-1} while the bottom panel includes those for Q=3 cm^{-3} s^{-1} . A value of 0.9 nm/h for GR used, as determined in Fig. 7 for this day. Negative and positive ion concentrations were assumed to be the same.